

Nonequilibrium Quasiparticle Dynamics in a MoRe-Based Superconducting Resonator under IR Excitation

O. A. Kalenyuk^{1,2} , S. I. Futimsky^{1,2} , I. A. Martynenko^{1,2} , A. P. Shapovalov^{1,2} ,

O. O. Boliasova^{1,2} , V. I. Shnyrkov^{1,2} , A. L. Kasatkin^{1,2} , A. A. Kordyuk^{1,2} 

AFFILIATIONS

¹G. V. Kurdyumov Institute for Metal Physics, N.A.S. of Ukraine, Kyiv, 03142, Ukraine

²Kyiv Academic University, Kyiv, 03142, Ukraine

^a)Author to whom correspondence should be addressed: oleksii.kaleniuk@gmail.com

ABSTRACT

The response of a MoRe-based superconducting resonator operating near 5 K to pulsed infrared irradiation is investigated, and the underlying physical mechanisms are analyzed. The device exhibits a pronounced nonlinear response dominated by nonequilibrium quasiparticle dynamics rather than uniform thermal heating. Infrared pulses produce strong distortions of the resonance curve and a transient decrease in the resonance frequency, consistent with increased kinetic inductance caused by quasiparticle generation. The frequency shift scales approximately linearly with absorbed power, whereas the dissipation response saturates at higher powers, indicating the formation of a nonequilibrium steady-state quasiparticle population. These observations demonstrate a transition from a linear pair-breaking regime to a saturated dissipation regime, likely associated with a quasiparticle relaxation bottleneck or partial suppression of the smaller superconducting gap in MoRe. The results highlight the relevance of nonequilibrium processes in MoRe and confirm its potential for microwave kinetic-inductance detector applications.

PACS numbers: 02.60.-x, 74.25.-q, 74.25.Nf, 74.70.-b, 74.78.-w.

Keywords: Microwave Kinetic Inductance Detectors (MKIDs), superconducting thin films, Hilbert fractal resonators, Infrared (IR) radiation, Molybdenum–Rhenium alloy.

I. INTRODUCTION

A wide variety of highly sensitive infrared (IR) detectors have been developed based on thin superconducting films. Two principal detection mechanisms are predominantly employed. The first relies on the bolometric effect, i.e., a sharp increase in the resistance of a narrow superconducting nanowire caused by the formation of a photon-induced hotspot. Such detectors are capable of resolving individual photons [1]. Their operation requires biasing the nanowire at a current close to the critical current and monitoring the onset of a finite voltage. This approach, however, necessitates a large number of electrical connections, particularly in the case of detector arrays. Additional drawbacks include the inability to detect radiation while the nanowire is in the normal state and the existence of a dead-time interval required for the system to recover its initial superconducting state. Thus, despite their excellent sensitivity, such detectors typically exhibit limited operational speed. The second approach is based on monitoring changes in the kinetic inductance of a superconducting film induced by photon absorption [2,3]. In this case, large arrays of superconducting resonators with distinct resonance frequencies are coupled to a single microwave feedline, significantly simplifying system architecture and enabling real-time two-dimensional imaging of incident electromagnetic radiation. The minimum detectable photon energy is determined by the superconducting energy gap, which in low-temperature superconductors is on the order of several meV. Kinetic-inductance detectors (MKIDs) have found extensive application in astrophysics, in particular for sky mapping at millimeter and sub-millimeter wavelengths [4]. Their operation, however, requires deep-cryogenic temperatures.

For a wide range of emerging applications—such as medical diagnostics, security systems, and detection of radiation in the terahertz and IR spectral ranges under high background illumination—the dynamic range and response speed are often more critical than ultimate sensitivity. In such cases, MKIDs operating at temperatures of a few kelvin may provide significant advantages. For example, Ref. [5] demonstrated the operating principles of a submillimeter-wave detector based on a superconducting kinetic-inductance thermometer at temperatures around 6 K.

Microwave kinetic inductance detectors (MKIDs) rely on thin films of low-temperature superconductors that provide high-quality resonators with a strong kinetic inductance contribution to the electrodynamic response. The most widely used materials include titanium nitride (TiN) [6], Ti/TiN multilayers, niobium nitride (NbN) [7], and aluminum (Al) [8], as well as their granular and composite modifications, all of which offer large superconducting energy gaps and stable device performance.

Recently, multiband superconductors, such as MgB_2 [9], have attracted significant interest, since the presence of multiple superconducting gaps can extend the dynamic range of detectable power and improve resilience to background radiation. These properties make such materials promising candidates for MKID applications in security systems, medical diagnostics, and terahertz photonics. Importantly, MoRe alloys have also been reported to exhibit signatures of multigap superconductivity [10-12], suggesting the coexistence of a small and a large superconducting gap. This multiband behavior makes MoRe a particularly appealing material for MKID development, as it may enable enhanced power-handling capability and improved performance under strong infrared illumination.

Another key requirement for practical detector arrays is device miniaturization, which is largely determined by the footprint of individual resonators. Fractal resonator geometries offer a promising route toward increasing the packing density, as they significantly reduce parasitic coupling between adjacent segments compared to traditional meander structures [13].

In our previous work, we investigated the response of a fractal MoRe superconducting resonator under continuous sinusoidal IR illumination [14]. In the present study, we examine the effect of pulsed IR radiation on the properties of a MoRe fractal resonator operating at 4.6 K.

II. EXPERIMENT

A fractal microstrip resonator with lateral dimensions of approximately $3 \times 3 \text{ mm}^2$ and a line width of $20 \mu\text{m}$ was fabricated from a 60 nm thick superconducting MoRe film deposited on a sapphire 0.5 mm substrate using standard photolithography. The topology of the resonator is shown in Fig. 1(a). The resonator was mounted on a copper sample holder and thermally anchored in helium vapor inside a 22-mm copper shield. As a source of infrared (IR) radiation, a miniature incandescent lamp was used and positioned 7.5 mm from the resonator [Fig. 1(b)]. The incandescent lamp provided a broadband IR source that could be positioned inside the compact copper shield without the need for external optical coupling, enabling direct measurements in a liquid-helium transport dewar. A similar configuration was employed in Ref. [14]. In the present configuration, a silicon wafer was placed between the lamp and the resonator to serve as an IR diffusing spectral filter. Since the glass envelope of the lamp blocks radiation at wavelengths longer than 4 μm [15], and silicon is opaque for wavelengths shorter than 1 μm , the resonator was irradiated within the spectral range 1–4 μm . The final sample mounting configuration is shown in Fig. 1(c). In contrast to Ref. [14], the continuous sinusoidal excitation of the lamp was replaced with short current pulses supplied directly to the incandescent filament from a pulse generator. During each pulse, the voltage across the lamp and the current through it were recorded, which enabled determination of the time dependence of the filament resistance. Comparison of this resistance evolution with a previously obtained calibration curve of filament resistance versus temperature [6] yielded the filament temperature time profile $T(t)$. Figure 1 (d) shows the resulting temperature dynamics for pulses of various durations, applied at a repetition rate of one pulse per second. Since the filament was operated in vacuum, its cooling occurred predominantly via thermal radiation. As a result, the filament did not fully cool down between pulses, and each subsequent pulse began at a temperature of approximately 400 K (see fig. 1 (d)). Thus, the preceding pulse established the initial conditions for the rapid heating of the filament during the next excitation. Figure 1 (e) shows the time dependence of the radiation power incident on the microstrip film, taking into account the filter

transmission, geometric factors, and the emissivity of the filament (details of the calculation are provided in Appendix A).

The resonator was implemented as a $\lambda/2$ open-ended fractal microstrip line segment (Fig. 1(a)) and was coupled to the external circuitry via symmetric capacitive coupling elements. The measurements were performed in a two-port configuration using a vector network analyzer. In this scheme, the complex transmission coefficient S_{21} — defined as the ratio of the output signal amplitude at *port 2* to the input signal amplitude applied at *port 1* — was recorded as a function of frequency f or time t .

In addition to the transmission coefficient, the insertion loss (IL) was evaluated, which characterizes the attenuation introduced by the resonator in the signal path. It is related to S_{21} by $IL = -20\log_{10}|S_{21}|$. Thus, the measurement set yields both the complex transmission response $S_{21}(f,t)$ and the corresponding insertion loss $IL(f,t)$, providing information about the resonant frequency, quality factor, and temporal dynamics of the resonator.

Superconducting fractal microstrip resonators exhibit a pronounced nonlinear response to microwave excitation power [16, 17]. Therefore, all measurements in this work were carried out in the linear regime, using a low probe power of -36 dBm (2.5×10^{-7} W).

III. RESULT AND DISCUSSION

Figure 1(f) shows a series of amplitude–frequency response curves of the resonator obtained under the influence of IR pulses repeated at a rate of one pulse per second during slow frequency scanning. The pulse duration was determined by the time during which current flowed through the incandescent filament of the lamp. As seen from the figure, pulses with a duration of 10 ms have virtually no effect on the shape of the resonance curve, which is consistent with the absence of significant radiated power during the first 10 ms of the pulse (Fig. 1(e)).

As the pulse duration increases, pronounced distortions of the resonance curve appear. During the pulse, sharp features are observed on the resonance profile, with their direction changing on the low- and high-frequency sides of the resonance. This behavior indicates a transient decrease in the resonance frequency at the moment of IR pulse excitation.

Next, the resonance frequency was fixed at $f=f_0$, and the parameter $S_{21}(t)$ was measured as a function of time t under the influence of the IR pulses. Figure 2(a) shows a series of such time traces obtained for different pulse durations. A pronounced decrease in S_{21} is observed during the interval in which current flows through the incandescent filament, followed by a slow relaxation. The latter is most likely associated with the continued IR irradiation while the filament cools down to a temperature of approximately 400 K (fig 1 e)).

Using the procedure described in Appendix B, the measured time dependence $S_{21}(t)$ was converted into the temporal variations of the resonance frequency $\Delta f_0(t)$ and the inverse internal quality factor $1/Q_0(t)$ (Figs. 2(b), 2(c)). In contrast to the resonance frequency shift, the inverse quality factor reaches saturation for pulse durations longer than approximately 70 ms.

Figure 2(d) shows the temperature dependences of the resonance frequency $f_0(T)$ and the inverse quality factor $1/Q_0(T)$, measured independently. By comparing these curves with the temporal dependences $\Delta f_0(t)$ and $1/Q_0(t)$, we determined the effective temperatures $T_f(t)$ and $T_Q(t)$ (Figs. 2(e), 2(f)). These results show that for a 10-ms IR pulse, the maximal effective temperature changes are $\Delta T_f=0.035$ K and $\Delta T_Q=0.87$ K at $P_s=340 \mu\text{W/mm}^2$.

In Ref. [18], it was reported that when a film on a sapphire substrate (as in our case) is illuminated with optical radiation at a power density of $P_s = 1 \text{ mW/mm}^2$, its temperature increases by $\Delta T \approx 0.1$ K. This estimate is fully consistent with our experimentally inferred frequency-based temperature change of $\Delta T_f \approx 0.036$ K at $P_s = 340 \mu\text{W/mm}^2$. At the same time, the dissipation-derived temperature shift ΔT_Q is much larger

than ΔT_f , demonstrating that the resonator response is dominated by non-equilibrium quasiparticle dynamics rather than by uniform thermal heating of the superconducting film.

In Appendix C we suggest an explanation of the observed dependences of the resonant frequency shift $\Delta f_0(P_s)$ and the resonator quality factor $\Delta(1/Q_0(P_s))$ on the incident radiation power as a result of the partial destruction of Cooper pairs and the creation of photoinduced quasiparticles, without taking into account the heating of the film.

Based on the temporal dependencies of $|S_{21}(t)|$, $\Delta f_0(t)$, and $1/Q_0(t)$ for $\tau=100$ ms (Fig. 2 a–c), as well as the absorbed power $P_s(t)$ (Fig. 1 e), the following dependences were evaluated: dissipation responsivity $\Delta(1/Q_0(P_s))=1/Q_0(P_s)-1/Q_0(0)$; frequency responsivity $\Delta(f_0(P_s))=f_0(0)-f_0(P_s)$; transmission amplitude responsivity $\Delta|S_{21}(P_s)|=|S_{21}(0)|-|S_{21}(P_s)|$ (fig. 3).

As shown in Fig. 3, the frequency responsivity $\Delta f_0(P_s)$ increases approximately proportionally with the incident IR power P_s , indicating a monotonic increase in the kinetic inductance due to quasiparticle generation. In contrast, the dissipation responsivity $\Delta(1/Q_0(P_s))$ becomes nearly independent of power for $P_s>250\mu\text{W}/\text{mm}^2$. This saturation behavior correlates with the time-domain evolution of the inverse quality factor in Fig. 2(c), suggesting the establishment of a nonequilibrium steady-state quasiparticle population, in which additional absorbed power does not lead to further microwave losses. A possible explanation for dependencies of this type for shifts in the resonant frequency and quality factor induced by the incident radiation power is given in Appendix C. The combined evolution of $\Delta f_0(P_s)$ and $\Delta(1/Q_0(P_s))$ results in a pronounced ΔS_{21} amplitude responsivity at low radiation powers, followed by a gradual decrease for $P_s>100\mu\text{W}/\text{mm}^2$. Such behavior is consistent with a transition from a linear pair-breaking regime to a saturated dissipation regime, which may be associated with a quasiparticle relaxation bottleneck or partial suppression of the smaller superconducting gap in MoRe.

IV. CONCLUSIONS

The resonator based on a MoRe superconducting film demonstrates a pronounced and nonlinear response to pulsed IR irradiation, governed primarily by nonequilibrium quasiparticle dynamics rather than by uniform thermal heating. Short IR pulses (10 ms) induce negligible changes in the resonance characteristics, consistent with the low radiated power during the initial heating stage of the filament. With increasing pulse duration and power, significant distortions of the resonance curve appear, reflecting a transient decrease in the resonance frequency due to enhanced kinetic inductance caused by quasiparticle generation.

Time-resolved measurements of $S_{21}(t)$, and their conversion into $\Delta f_0(t)$ and $1/Q_0(t)$, reveal fundamentally different behaviors for frequency shift and dissipation. While the resonance frequency shift scales approximately linearly with absorbed power, the inverse quality factor exhibits clear saturation for higher powers and longer pulse durations. This indicates the formation of a nonequilibrium steady-state quasiparticle population, in which further increases in absorbed power do not result in additional microwave losses.

The effective temperature analysis confirms that the dissipation-derived temperature rise significantly exceeds the frequency-derived temperature change, providing strong evidence that the detector response is dominated by quasiparticle pair-breaking processes rather than simple thermal effects. The observed saturation of dissipation responsivity and the reduction of transmission amplitude responsivity at higher powers suggest a transition from a linear pair-breaking regime to a saturated regime, likely associated with a quasiparticle relaxation bottleneck or partial suppression of the smaller superconducting gap in MoRe.

Overall, the results highlight the suitability of MoRe-based resonators for detecting IR radiation via kinetic inductance effects and underline the importance of nonequilibrium processes in defining their responsivity and dynamic range. These findings are also consistent with the presence of multigap superconductivity in MoRe, which may play a key role in the observed nonlinear response characteristics.

Acknowledgments

This research was carried out within the framework of the project 2023.04/0157 funded by the National Research Foundation of Ukraine «High-speed matrix kinetic detector of long-wave infrared radiation».

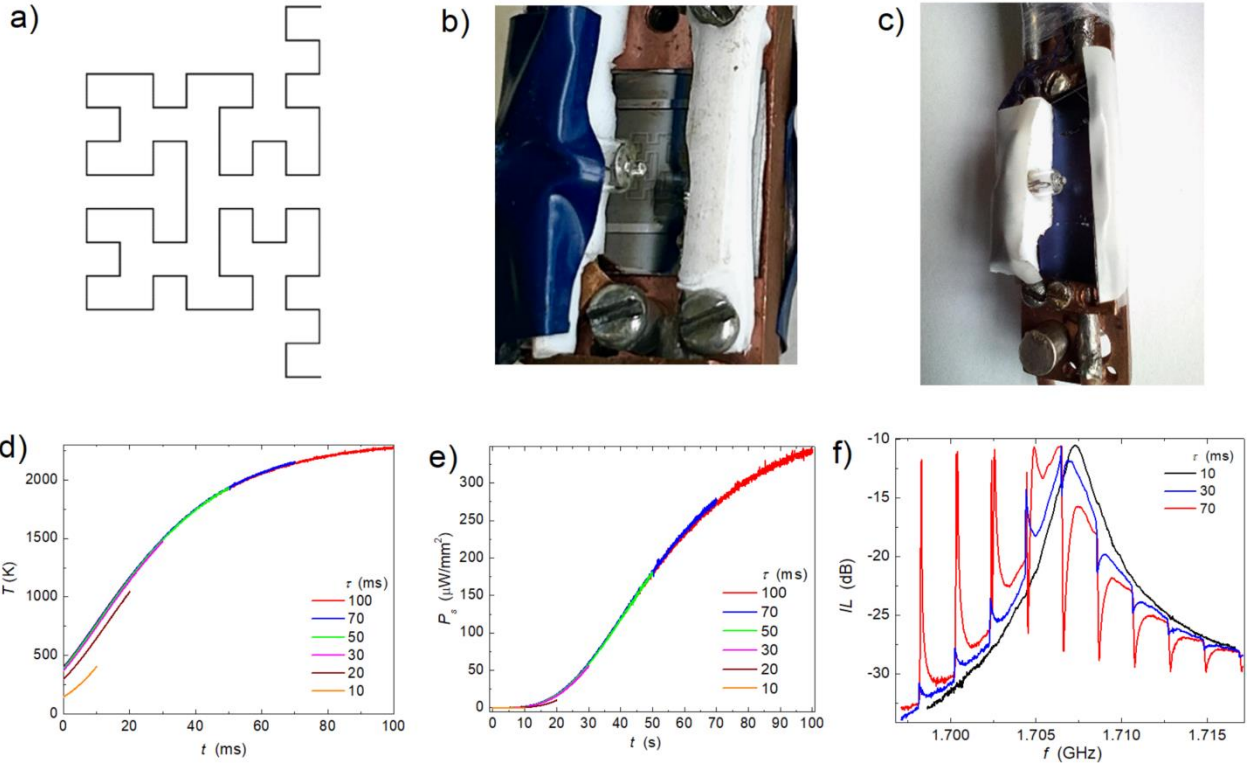


Fig. 1. Topology of the fractal resonator (a). MoRe resonator mounted on a copper sample holder (b). General view of the holder with a silicon wafer IR filter positioned between the resonator and the incandescent lamp (c). Temperature of the incandescent filament T for pulses of different durations (d). IR power incident on the resonator P_s (e). Series of amplitude–frequency response characteristics IL measured under IR pulses of varying duration (f).

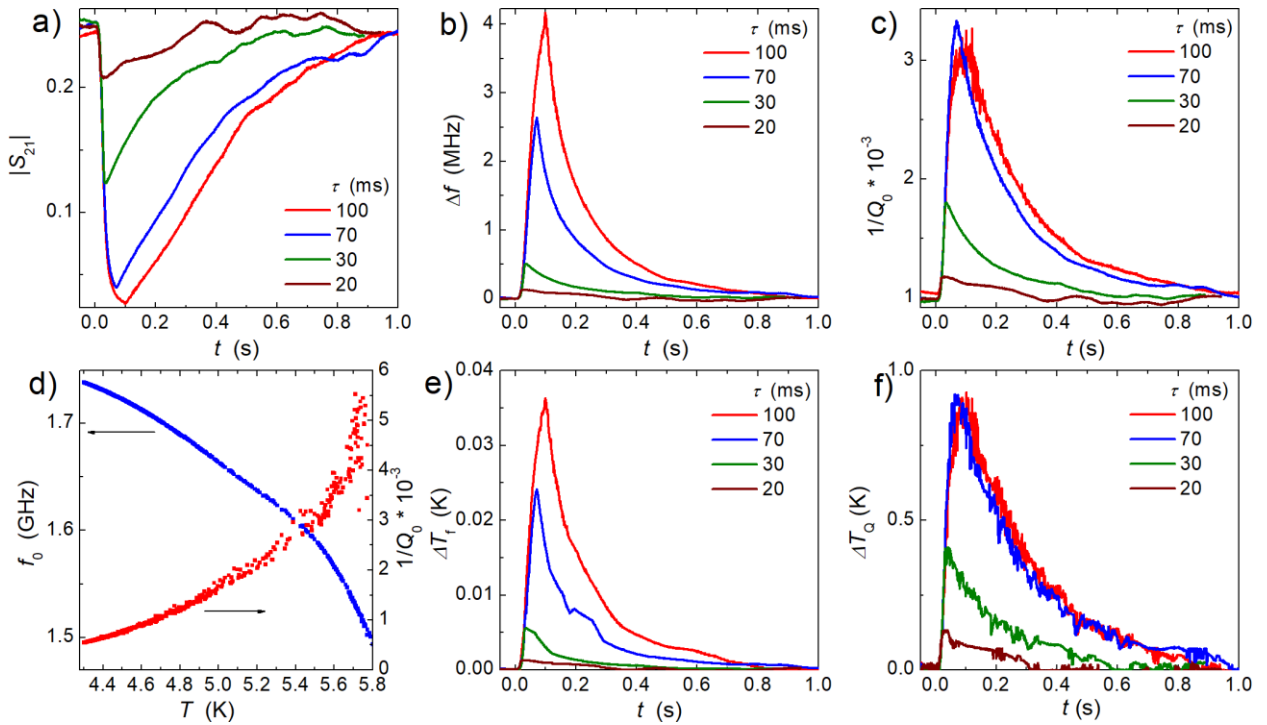


Fig. 2. IR pulse amplitude response $|S_{21}|$ (a), resonance frequency shift Δf (b), inverse quality factor $1/Q_0$ (c). Temperature dependences of the resonance frequency f_0 and inverse quality factor $1/Q_0$ (d), and effective temperature rises derived from the resonance frequency shift ΔT_f (e) and from the variation of the quality factor ΔT_Q (f).

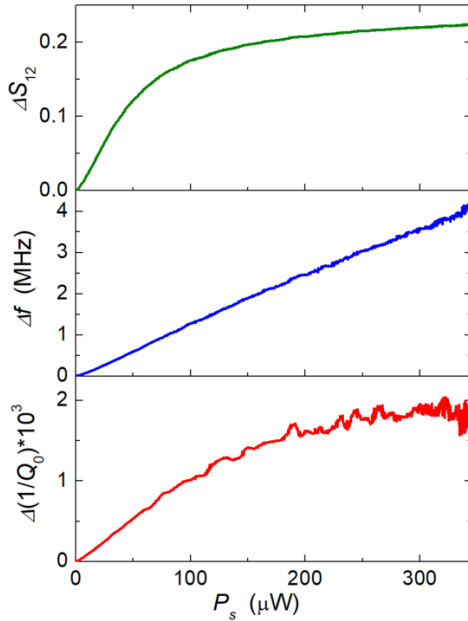


Fig. 3. IR power amplitude ΔS_{21} , frequency Δf_0 and dissipation $\Delta(1/Q_0)$ responsivities.

APPENDIX A: RADIATION POWER

To determine the emitted radiation power, the temperature function $T(t)$ was substituted into Planck's law expression for the spectral radiance of an ideal blackbody. The power emitted per unit surface area in the wavelength interval $[\lambda_1, \lambda_2]$ was calculated as

$$P(\lambda_1, \lambda_2, T) = \int_{\lambda_1}^{\lambda_2} \frac{2\pi hc^2}{\lambda^5} \frac{1}{\exp\left(\frac{hc}{\lambda k_B T}\right) - 1} d\lambda,$$

where λ is the wavelength, h is Planck's constant, c is the speed of light, and k_B is Boltzmann's constant. Using this expression, the time dependence of the emitted power in the spectral range 1–4 μm was obtained as a function $P(t)$.

To estimate the radiation power incident at the superconducting microstrip line, we write

$$P_s(t) = S_f \cdot \varepsilon \cdot \frac{1}{S_d} \cdot k_f \cdot P(t) = k \cdot P(t)$$

where $S_f=1.3\times10^{-6}$ m² is the area of the incandescent filament, $\varepsilon\approx0.35$ is the emissivity of tungsten, $S_d=7.07\times10^{-4}$ m² is the surface area of a sphere with radius equal to the distance between the lamp and the resonator $d=7.5$ mm, and k_f is the transmission coefficient of the optical glass-silicon filter.

In the wavelength range 1–4 μm, both silicon and the glass envelope of the lamp are transparent; therefore, the dominant losses are associated with reflections at the vacuum–glass and vacuum–silicon interfaces. The glass envelope absorbs up to 10% of the emitted power [15]. Due to the high refractive index of silicon ($n\approx3.42$), reflection at the two silicon–vacuum interfaces result in radiation losses of approximately 50%. Thus, the overall transmission coefficient is $k_f\approx 0.45$.

Substituting the values S_f , S_d , ε and k_f gives $k = 2.9\times10^{-10}$.

APPENDIX B: RESONATOR TRANSMISSION MODEL

Near resonance, the transmission S_{12} of a weakly coupled, symmetric two-port resonator can be written in the standard Lorentzian (input–output) form

$$S_{12}(\omega) = \frac{2\gamma_e}{\gamma_{tot} - 2j(\omega - \omega_0)}, \quad (B1)$$

where $\omega_0=2\pi f_0$ is the instantaneous resonant angular frequency,

$$\gamma_{tot} = \gamma_i + 2\gamma_e \quad (B2)$$

is the total decay rate - internal γ_i plus two equal external channels decay rate $2\gamma_e$. The factor 2 in the numerator arises from the symmetric contribution of two couplers. The denominator $\gamma_{tot} - 2j(\omega - \omega_0)$ reflects damping and detuning of the resonant mode. At resonance $\omega = \omega_0$, in accordance with formula (B1) we obtain:

$$\gamma_e = \frac{S_{12}(\omega_0)}{2} \gamma_{tot}(\omega_0). \quad (B3)$$

The total decay rate γ_{tot} is determined by the loaded quality factor Q_{L0} :

$$\gamma_{tot}(\omega_0) = \frac{\omega_0}{2Q_{L0}}. \quad (B4)$$

The external channels decay γ_e can be found by formulas (B3) and (B4):

$$\gamma_e = \frac{S_{12}(\omega_0)}{2} \frac{\omega_0}{2Q_{L0}}. \quad (B5)$$

If the resonant frequency $\omega(t)$ and the total decay rate $\gamma_{tot}(t)$ vary over time t , while the measurements of $S_{21}(t)$ are performed at a fixed probing frequency ω_0 , then equation (B1) can be rewritten as:

$$\frac{1}{S_{21}(t)} = \frac{\gamma_{tot}(t)}{2\gamma_e} - j \frac{\omega_0 - \omega(t)}{\gamma_e}. \quad (B6)$$

By separating the real and imaginary parts of equation (B6), we obtain the expressions for determining the time-dependent functions $\gamma_{tot}(t)$ and $\Delta\omega(t)$:

$$\gamma_{tot}(t) = 2\gamma_e \Re\left[\frac{1}{S_{21}(t)}\right], \quad (B7)$$

$$\Delta\omega(t) = \omega_0 - \omega(t) = -\gamma_e \Im\left[\frac{1}{S_{21}(t)}\right]. \quad (B8)$$

In the approximation $\omega \approx \omega_0$, equation (4) yields expressions for determining the loaded quality factor $Q_L(t)$ and the unloaded quality factor $Q_0(t)$:

$$Q_L(t) = \frac{\omega_0}{2\gamma_{tot}(t)}, \quad (B9)$$

$$\frac{1}{Q_0(t)} = \frac{1}{Q_L(t)} - \frac{4\gamma_e}{\omega_0} \quad (10)$$

APPENDIX C: DEPENDENCIES OF THE RESONANCE FREQUENCY AND SURFACE RESISTANCE ON THE INCIDENT LIGHT POWER

Here we analyze dependencies of the resonance frequency f_0 and the inverse quality factor $1/Q_0$ of the resonator under study on the incident radiation power P_s . We assume that the reason for these dependencies is related to the breaking of Cooper pairs in the superconductor by absorbed photons in the incident light with an energy above the threshold value 2Δ (Δ is the gap in the quasiparticles energy spectrum in a superconductor).

The resonant frequency f_0 is determined by the well-known formula $f_0 = 1/\sqrt{LC}$, where L and C are the characteristic inductance and capacitance of the resonator. For the superconducting thin film with a

thickness $d \ll \lambda_L$ (λ_L is the London penetration depth, $\lambda_L \sim 300\text{nm}$) one has for the kinetic inductance of the superconducting film $L \approx L_k = \mu_0 \left(\lambda_L^2 / d \right)$ (see, e. g. [19]). This is just the case of our experiment. In the framework of the two-fluid model for superconductivity the London penetration depth is given by the relation: $\lambda_L^2(T) = \frac{m}{\mu_0 e^2 n_s(T)}$, where n_s - is the superfluid electron density, e - is the electron charge and m - is the electron mass.

Under the influence of light irradiation with a frequency above the threshold: $\hbar\omega > 2\Delta$, the destruction of Cooper pairs occurs and, accordingly, nonequilibrium quasiparticles (which are 'normal electrons' in the two-fluid model) are formed with a concentration n_{ex} , the value of which is proportional to the absorbed light power P_s , as follows from the simplest dynamic equation: $\frac{dn_{ex}}{dt} = I_0 - \frac{n_{ex}}{\tau_r}$, where I_0 is the rate of quasiparticle generation by absorbed light: $I_0 = \kappa P_s$ (κ is a numerical coefficient), τ_r is the recombination time.

In the steady-state regime, $\frac{dn_{ex}}{dt} = 0$, and $n_{ex} = I_0 \tau_r = \kappa P_s \tau_r$, i.e., the concentration of nonequilibrium quasiparticles is quite clearly proportional to the absorbed irradiation power P_s (assuming that τ_r is independent on P_s). According to the two-fluid model of a superconductor, such irradiation with a frequency above the threshold value should lead to a decrease in the concentration of superfluid electrons: $n_s \rightarrow n_s - n_{ex}$. Correspondingly, changes in the London depth, kinetic inductance, and resonant frequency occur:

$$\lambda_L^2 = \frac{m}{\mu_0 e^2 (n_s(T) - n_{ex})} = \lambda_L^2(T) \left[1 + \frac{n_{ex}}{n_s(T)} \right] = \lambda_L^2(T) + \Delta(\lambda_L^2); \Delta(\lambda_L^2) = \lambda_L^2(T) \frac{n_{ex}}{n_s(T)} \quad (C1)$$

$$L_k = \mu_0 \left(\lambda_L^2 / d \right) = L_k(T) + \Delta(L_k); \Delta(L_k) = \mu_0 \left(\frac{\Delta(\lambda_L^2)}{d} \right) = L_k(T) \frac{n_{ex}}{n_s(T)}; \quad (C2)$$

$$f = 1/\sqrt{LC} = 1/\sqrt{(L_k(T) + \Delta(L_k))C} = 1/\sqrt{L_k(T)C \left[1 + \frac{n_{ex}}{n_s(T)} \right]} \cong f_0(T) \left(1 - \frac{n_{ex}}{n_s(T)} \right); \quad (C3)$$

$$\Delta f = f - f_0(T) = -f_0(T) \left(\frac{n_{ex}}{n_s(T)} \right) = -f_0(T) \left(\frac{\kappa P_s \tau_r}{n_s(T)} \right) \propto P_s. \quad (C4)$$

Thus, the shift in the resonant frequency is approximately proportional to the power of the incident light radiation in accordance with our experimental data (see Fig.3).

An explanation of the experimental dependence of the resonator inverse quality factor $1/Q_0$ on the light irradiation power P_s , shown in Fig. 3, requires a more in-depth analysis of the kinetics of irradiation-excited quasiparticles and their recombination. We will rely on the phenomenological model of Rothwarf and Taylor [20], subsequently developed and supplemented in [21-22].

The value of $1/Q_0$ determines the value of the superconductor surface resistance in the microwave range [23]: $\frac{1}{Q_0} \propto R_s \propto \sigma_1$, where σ_1 is the real part of the high-frequency conductivity, proportional, according to the Drude formula, to the concentration of normal electrons. Therefore, a change in the concentration of normal electrons due to nonequilibrium quasiparticles induced by incident light leads to a change in the quality factor of the resonator: $\Delta \left(\frac{1}{Q_0} \right) \propto \Delta \sigma_1 \propto n_{ex}(P_s)$.

The phenomenological model approach, based on the work of Rothwarf and Taylor [20], allows us to understand and explain the observed effect of saturation on the dependence of $\Delta \left(\frac{1}{Q_0} \right)$ on the incident light power P_s , as shown in Fig. 3.

The equations for the dynamics of nonequilibrium quasiparticles and phonons in a single-band superconductor exposed to light with a frequency $\omega > 2\Delta/\hbar$, within the framework of the phenomenological model of Rothwarf and Taylor [20], have the form:

$$\frac{dn_n}{dt} = I_0 - R n_n^2 + \beta N_\omega; \quad (C5)$$

$$\frac{dN_\omega}{dt} = R \frac{n_n^2}{2} - \beta \frac{N_\omega}{2} - \frac{N_\omega - N_{\omega,th}}{\tau_\gamma} \quad (C6)$$

where n_n is the total concentration of quasiparticles: $n_n = n_n(T) + n_{ex}$, $I_0 = \kappa P_s$ is normalized incident power (see above), R is the recombination coefficient, N_ω is the total number of phonons with energy $\hbar\omega > 2\Delta$, β is the transition probability for the breaking of Cooper pairs by such phonons, and the $1/\gamma$ is the transition probability for phonons to escape from the energy range $\hbar\omega > 2\Delta$ by processes other than pair breaking. In the stationary case: $\frac{dn_n}{dt} = \frac{dN_\omega}{dt} = 0$, the solution of equations (C5), (C6) for the concentration of quasiparticles $n_n = n_n(T) + n_{ex}$ takes the form [20]:

$$n_n = \left[\frac{\beta N_{\omega,th} + I_0 \left(1 + \frac{\beta}{2} \tau_\gamma \right)}{R} \right]^{1/2} \quad (C7)$$

From (C7) it follows that in the absence of IR irradiation ($I_0=0$) the equilibrium concentration of quasiparticles $n_n(T)$ equals $\left[\frac{\beta N_{\omega,th}}{R} \right]^{1/2}$. It also follows from expression (C7) that for finite values of the incident irradiation power, the dependence of the concentration of photoinduced quasiparticles $n_{ex}(I_0)$ depends linearly on I_0 at low excitation levels, and at high values of I_0 , this dependence changes to a flatter, square root dependence: $n_{ex}(I_0) \sim (I_0)^{1/2} = (\kappa P_s)^{1/2}$. This is in good agreement with the experimental results presented in Fig. 3, since, as noted above, $\Delta \left(\frac{1}{Q_0} \right) \propto \Delta \sigma_1 \propto n_{ex}(P_s)$. The possible saturation effect of the dependence $\Delta \left(\frac{1}{Q_0} \right)$ on the irradiation power at high values of P_s can be due to the so-called effect of phonon bottleneck [21,22]. The latter corresponds to a regime in which the recombination of nonequilibrium quasiparticles is significantly slowed down due to the accumulation of high-energy phonons, which repeatedly break Cooper pairs.

REFERENCES

¹ C. M. Natarajan, M. G. Tanner, and R. H. Hadfield, “Superconducting nanowire single-photon detectors: physics and applications,” *Supercond. Sci. Technol.* **25** (6), 063001 (2012).

² P. K. Day, H.G. LeDuc, B. A. Mazin, A. Vayonakis, and J. Zmuidzinas, “A broadband superconducting detector suitable for use in large arrays,” *Nature* **425**, 817–821 (2003).

³ G. Ulbricht, M. De Lucia, and E. Baldwin, “Applications for Microwave Kinetic Induction Detectors in Advanced Instrumentation,” *Appl. Sci.* **11**(6), 2671 (2021).

⁴ N. Boudou, A. Benoit, O. Bourrion, M. Calvo, F.-X. Désert, J. Macias-Perez, A. Monfardini, M. Roesch, “Kinetic inductance detectors for millimeter and submillimeter astronomy,” *C. R. Phys.* **13** (1), 62-70 (2012).

⁵ A.V. Timofeev, V. Vesterinen, P. Helistö, L. Grönberg, J. Hassel, and A. Luukanen, “Submillimeter-wave kinetic inductance bolometers on free-standing nanomembranes,” *Supercond. Sci. Technol.* **27** (2), 025002 (2013).

⁶ D. Morozov, S.M. Doyle, A. Banerjee, T. L. R. Brien, D. Hemakumara, I. G. Thayne, K. Wood and R. H. Hadfield, “Design and Characterisation of Titanium Nitride Subarrays of Kinetic Inductance Detectors for Passive Terahertz Imaging,” *J. Low Temp. Phys.* **193**, 196–202 (2018).

⁷ K. Hayashi, A. Saito, Y. Ogawa, M. Murata, T. Sawada, K. Nakajima, H. Yamada, S. Ariyoshi, T. Taino, H. Tanoue, C. Otani, and S. Ohshima, “Design and Fabrication of Microwave Kinetic Inductance Detectors using NbN Symmetric Spiral Resonator Array,” *J. Phys.: Conf. Ser.* **507**, 042015 (2014).

⁸ T. Noguchi; A. Dominjon, Y. Sekimoto, “Analysis of Characteristics of Al MKID Resonators,” *IEEE Trans. Appl. Supercond.* **28** (4), 2400206 (2018).

⁹ A. Roitman, C. Pfaff, T. Hauet, A. Shaulov, and Y. Yeshurun, “Microwave Kinetic Inductance Detector Made of Molecular Beam Epitaxy (MBE)-Grown MgB₂ Film,” *Nanomaterials* **14** (21), 1731 (2024).

¹⁰ S. Sundar, L. S. S. Chandra, M. K. Chattopadhyay, S. K. Pandey, D. Venkateshwarlu, R. Rawat, V. Ganesan, and S. B. Roy, “Strong electron–phonon coupling and multiband effects in the superconducting β -phase $\text{Mo}_{1-x}\text{Re}_x$ alloys,” *New J. Phys.* **17**, 053003 (2015).

¹¹ A. D'yachenko, A. Kalenyuk, V. Tarenkov, A. Shapovalov, O. Boliasova, D. Menesenko, “Spectroscopy of electron-phonon interaction in β phase of Mo-Re alloy,” *Low Temp. Phys.* **49**, 209–215 (2023).

¹² A. Kalenyuk, A. Shapovalov, V. Shnyrkov, V. Shaternik, M. Belogolovskii, P. Febvre, F. Schmidl, and P. Seidel, “Submicron-sized MoRe-doped Si-MoRe Josephson junctions with a low specific capacitance,” *J. Phys.: Conf. Ser.* **1559**, 012005 (2020).

¹³ A. A. Kalenyuk, S. I. Futimsky, “Miniature meander- and fractal-shaped microstrip resonators,”, *Metallofiz. Noveishie Tekhnol.* **40**, 1573 (2018).

¹⁴ O. A. Kalenyuk, S. I. Futimsky, I. A. Martynenko, A. P. Shapovalov, V. I. Shnyrkov, A. A. Kordyuk, “Development of microwave kinetic inductance detectors suitable for fast infrared thermography,” *Low Temp. Phys.* **51**, 1374–1379 (2025).

¹⁵ M. Dauphin, S. Albin, M. El-Hafi, Y. Le Maoult, F. M. Schmidt, “Towards thermal model of automotive lamps,” in Proceedings of the *11 international conference on Quantitative Infrared Thermography* (Naples, Italy, 2012), p. 10, see <http://dx.doi.org/10.21611/qirt.2012.262>

¹⁶ A. A. Kalenyuk, T. Golod, A. P. Shapovalov, A. L. Kasatkin, S. I. Futimsky, “Nonlinear Properties of Superconducting Microstrip Hilbert Fractal Resonators,” in Proceedings of the *2020 IEEE Ukrainian Microwave Week (UkrMW)*, Kharkiv, Ukraine (2020), p. 743, see <https://doi.org/10.1109/UkrMW49653.2020.9252756>

¹⁷ O. A. Kalenyuk, S. I. Futimsky, A. P. Shapovalov, “Nonlinear response of superconducting (YBCO) fractal microstrip resonators: Distributed current ABCD-matrix model,” *AIP Adv.* **15**, 025035 (2025).

¹⁸ C. Kurter, A. P. Zhuravel, A. V. Ustinov, and S. M. Anlage, “Microscopic examination of hot spots giving rise to nonlinearity in superconducting resonators,” *Phys. Rev. B* **84**, 104515 (2011).

¹⁹ V.V. Shmidt, *The Physics of Superconductors: Introduction to Fundamentals and Applications* (Springer Science & Business Media, 2013).

²⁰ A. Rothwarf and B. N. Taylor, "Measurement of Recombination Lifetimes in Superconductors," *Phys. Rev. Lett.* **19**, 27 (1967).

²¹ J. Demsar, R. D. Averitt, A. J. Taylor, V.V. Kabanov, W. N. Kang, H. J. Kim, E. M. Choi, and S. I. Lee, "Pair-Breaking and Superconducting State Recovery Dynamics in MgB₂," *Phys. Rev. Lett.* **91**, 267002 (2003).

²² V. V. Kabanov, J. Demsar, and D. Mihailovic, "Kinetics of a Superconductor Excited with a Femtosecond Optical Pulse," *Phys. Rev. Lett.* **95**, 147002 (2005).